Sheet-flow Sediment Transport under Nonlinear Oscillatory flow over a sloping bed

Weikai Tan[a], Jing Yuan[a]

[a]*Department of Civil and Environmental Engineering, National University of Singapore, 1 Engineering Dr. 2, Block E1A 07-03, Singapore 117576*

Abstract

Seabed is usually sloped in shallow coastal regions, where strong nonlinear shoaling waves can generate sheet-flow sediment transport. Both wave nonlinearity and bottom slope can lead to wave-averaged (net) sediment transport rate, but the latter is often overlooked in existing models. A full-scale experimental study of sheet-flow sediment transport under oscillatory flows with nonlinear features (skewness or asymmetry) was conducted in an inclinable oscillatory water tunnel, so bottom-slope-induced net transport rate in the context of nonlinear waves was experimentally investigated. The tests cover a variety of nonlinear wave shape, bottom slope (0 to 2.5°) and two sediment diameters (0.24 and 0.51 mm). Since the downslope direction is the "offshore" direction in our tests, it is found that bottom slope reduces the net "onshore" transport rate due to wave nonlinearity. The slope's contribution in net transport rate is evaluated by taking the difference between a sloping-bed test and its corresponding horizontal-bed test. The results suggest that slope-induced net transport rate is insensitive to wave nonlinearity, and its variation with bottom slope can be considered linear in the context of predicting net transport rate. Comparisons between this study and a preceding

sinusoidal-flow study of Yuan et al. (2017b) suggest that nonlinear waves can be approximated as sinusoidal flows for evaluating modeling slope's contribution in net transport rate. Subsequently, an empirical model for predicting net sheet-flow transport rate due to bottom slope is established based on dimensional analysis. This model can be simply added to existing sheet-flow sediment transport models to improve their applicability in coastal regions.
Keywords: sheet flow, sediment transport, bottom slope, experimental study, empirical formula

1. Introduction

Modeling net sediment transport rate under shoaling waves in coastal regions is a challenging topic in coastal engineering, which is mainly due to the complexity of associated physical process. Sediment transport in the sheet-flow regime, which is referred to intense sediment motion concentrated within a very thin layer above a dynamically flat bed, has gained extensive attention in recent years. This is mainly because sheet-flow sediment transport can occur in very shallow waters, e.g., within the surf zone, and therefore is directly related to coastal erosion or other important coastal processes.

Wave nonlinearity is believed to be the main reason for a net wave-averaged sheet flow sediment transport rate. As waves propagate into shallow water, the two half-cycles of the near-bottom orbital velocity becomes different. The onshore half-cycle has a shorter duration but a larger crest value than the offshore half-cycle, which is referred to as skewness. Also, the time series of bottom orbital velocity becomes forward-leaning (or has a saw-tooth shape), which is conventionally named as asymmetry. Skewness can be

expected to produce an onshore net transport rate based on a simple quasi-steady consideration, which assumes that instantaneous transport rate q has a power-law dependency on near-bed velocity u_∞ (e.g. $q \sim u_\infty^3$) (e.g. Madsen and Grant, 1977; Bailard, 1981). For asymmetry, Nielsen (1992) argued that wave boundary layer has less time to develop during the rapidly accelerating half-cycle, which enhances the instantaneous bottom shear stress, so a quasi-steady argument can also lead to a net onshore transport rate, which is confirmed by some experiments (e.g. Watanabe and Sato, 2004; O'Donoghue and Wright, 2004). Since bedload transport can be modeled in a quasi-steady manner due to the very short responding time of sediment grain, a few quasi-steady models (e.g. Ribberink, 1998; Gonzalez-Rodriguez and Madsen, 2007; Wang, 2007) have been proposed, and they work well for coarse-sand scenarios. However, such quasi-steady models do not work for experiments in oscillatory water tunnels (OWT) with fine sediment grains. For example, Ribberink and Al-Salem (1995) showed that the net onshore transport rate due to skewness increases with wave period, while O'Donoghue and Wright (2004) obtained offshore net sheet-flow transport rate for skewed oscillatory flows over fine-sand bed. These experiments lead to the argument of a phase-lag effect (see Dohmen-Janssen et al., 2002), i.e., sediment suspended during one half-cycle cannot immediately settle back to the bed before flow reversal and is subsequently transported in the next half-cycle. This argument is supported by intra-period measurements of velocity and sediment concentration, e.g., Ribberink and Al-Salem (1995) and O'Donoghue and Wright (2004). The phase-lag effect is also present for asymmetric oscillatory flow. According to recent OWT experiments (e.g. Ruessink et al., 2011), sedi-

ment grains suspended during the offshore half-cycle has less time to settle than those suspended during the onshore half-cycle, since velocity asymmetry shortens the reversal from negative to positive half-cycle. As a result, phase-lag effect increases the onshore net transport rate for asymmetric oscillatory flows. With a large dataset of full-scale experiments (see Van der Werf et al., 2009), some empirical formulas that include the phase-lag effect have been proposed (e.g. da Silva et al., 2006; van der A et al., 2013). Another physics that can lead to a net transport rate is wave boundary layer streaming, which can be produced by longitudinal variation of boundary layer flow associated with wave propagation (c.f. Longuet-Higgins, 1953) or a nonlinear wave shape (see Trowbridge and Madsen, 1984). The reader is referred to Kranenburg et al. (2012) and Yuan and Madsen (2015) for in-depth literature review. The effect of boundary layer streaming associated with wave propagation has also been added in recent empirical models for coastal sediment transport (see van der A et al., 2013).

In terms of modeling net sheet-flow sediment transport in a process-based manner, a substantial amount of theoretical or numerical studies have been reported in the past decays. Many models adopt the one-phase approach, which considers sediment as passive substances. These models solve the Reynolds-averaged Navier-Stokes equation for boundary layer flow, and the convection-diffusion equation for sediment concentration. The major difference among these models is the turbulence closure model, i.e., one-equation (e.g. Davies and Li, 1997; Davies et al., 1988) or two-equation closures (e.g. Ruessink et al., 2009; Hassan and Ribberink, 2010; Fuhrman et al., 2013; Caliskan and Fuhrman, 2017). The drawback of one-phase model is

that it cannot directly resolve the sheet-flow layer, i.e., a rather artificial separation of bedload and suspended-load layers must be adopted. As a more advanced numerical method, two-phase model (e.g. Hsu et al., 2004; Liu and Sato, 2006; Chen et al., 2011) has been applied for sheet-flow sediment transport, which treats the sediment and water as two continuous mediums and models the inter-phase stresses. Compared to one-phase models, two-phase models are still in the infancy stage, and many research efforts are required for further improving closure models for inter-phase stresses and enhancing computational efficiencies. Nevertheless, these numerical models are valuable tools for complementing experimental results.

Bottom slope is another essential factor for net sediment transport rate in the coastal environment, which, however, is not that well studied. King (1991) conducted OWT measurements of sediment transport rate under half-cycle of sinusoidal flow with different bottom slopes. He found a linear relationship between half-cycle-average sediment transport rate and bottom slope. However, using separated half-cycles to approximate the net sediment transport under sinusoidal oscillatory flow can be questionable, e.g., the aforementioned phase-lag effect may be excluded. Recently, Yuan et al. (2017b) (YLM17 hereafter) conducted sheet-flow experiments of sinusoidal oscillatory flows over a sloping bed in OWT. With a sinusoidal wave shape, the net transport rate is purely due to bottom slope. They found that the net transport rate is in the downslope direction and increases linearly with bottom slope. They argued that during the downslope half-cycle a bottom-parallel gravity force increases the total bedload transport. Consequently, sediment suspension and hence the total suspended-load transport is also

increased for the downslope half-cycle. The opposite occurs for the upslope half-cycle. As a result, a net downslope sheet-flow transport rate is produced. They subsequently developed a conceptual model based on these arguments, which agrees well with their measurements. Following this work, Yuan and Tan (2018) developed a theoretical model that can predict net sheet-flow sediment transport rate for oscillatory flows with nonlinear wave shapes over a sloping bed. Through some case studies with this model, they found that the bottom-slope effect can be as important as nonlinear wave shape effects (i.e. skewness and asymmetry).

One implication of Yuan and Tan (2018) model is that the net transport rates due to bottom slope and wave nonlinearity can be modeled separately. One can model nonlinear wave shape effect by ignoring bottom slope and model slope effect by only considering an equivalent sinusoidal oscillatory flow. The total transport rate can be obtained by simply adding the two effects. If this is true, one can easily add bottom-slope effect into any previous models which only work for horizontal beds. Obtaining experimental evidence that supports this implication is the primary target of this paper. To this end, we conducted sheet-flow tests in an OWT, in which skewed or asymmetric oscillatory flows are produced over sloping bottoms. The outline of this paper is as follow. In section 2, we present the experimental facility and experimental methodology. Section 3 discusses the experimental results. An empirical formula, which predicts net sheet-flow transport rate due to bottom slope, is introduced in section 4. Conclusions are provided in section 5.

2. Experimental conditions

In this study, full-scale experiments of sheet-flow sediment transport under oscillatory flows over sloping beds are performed in an oscillatory water tunnel. The target oscillatory flows are skewed or asymmetric, so net sediment transport rate is due to both wave nonlinearity and bottom slope. In this section, we introduce the experimental facility, test condition and the determination of net sediment transport rate.

2.1. Experimental facility and instrument

The main facility is an OWT in the Hydraulic Engineering Laboratory of National University of Singapore. This OWT is also named Wave-Current-Sediment (WCS) facility. It consists of a 10 m-long enclosed horizontal test channel with a rectangular cross section (40 cm wide and 50 cm deep) and two vertical cylindrical risers at the ends of the test channel (see Fig. 1). One riser is open to the air and the other houses a hydraulic-driven piston, so oscillatory flow in the channel can be generated by the oscillatory movement of piston. The facility is mainly supported by a pivot near the piston end and a hydraulic jack at the open-riser end, so the test channel can be tilt to give a bottom slope up to 2.6°. Preliminary study by Yuan and Madsen (2014) confirmed that the WCS can produce specified oscillatory flows very precisely.

Net sediment rate in the test section is measured with a laser-based bottom profiler (LBP) system through the principle of sediment volume conservation (see section 2.3 for details and examples). The LBP system measures the change of bottom profile. Two red laser sheets are vertically introduced

into the test section through the transparent acrylic lid of the test section, so two longitudinal laser lines following the movable bottom are produced. The red laser lines are symmetrically located on the two sides of the test channel's lateral centreline (with 1/4 channel width from the centreline), and can be well captured by digital cameras in a dark environment. By tracking the vertical displacements of laser lines on digital image, the change of bottom profile Δz_b can be accurately determined. The readers are referred to Yuan et al. (2017a) for more details about the LBP.

2.2. Test conditions

All tests in this study have periodic oscillatory flows which consist of two harmonics, i.e.

$$U_\infty(t) = U_{1\infty}[cos(\omega t) + \alpha cos(2\omega t + \varphi_0)] \tag{1}$$

where $U_{1\infty}$ is the amplitude of first-harmonic velocity, $\alpha < 1$ is the relative size of second harmonic, $\omega = 2\pi/T$ is the radian frequency with T being the flow period, φ_0 is the relative phase of second harmonic (0° for pure skewness and 90° for pure asymmetric). To ensure sheet-flow condition, the following Shields-parameter criterion for sinusoidal oscillatory flow,

$$\psi_{wmd} = \frac{f_{wd} U_{bm}^2}{2(s-1)g d_{50}} > 0.7 \tag{2}$$

proposed by Madsen (1993), is adopted, where g is gravitational acceleration, s is sediment specific density, d_{50} is sediment median diameter, U_{bm} is the maximum free-stream velocity and ψ_{wmd} is the characteristic Shields parameter. The wave friction factor f_{wd} in Eq. (2) is determined by the formula

proposed by Humbyrd (2012), i.e.

$$f_{wd} = exp\left[5.70\left(\frac{A_{bm}}{k_b}\right)^{-0.101} - 7.46\right], 10 \leq \frac{A_{bm}}{k_b} \leq 10^5 \tag{3}$$

where $A_{bm} = U_{bm}/\omega$ is the excursion amplitude and the bottom roughness k_b is taken as $k_b = d_{50}$. Since the first-harmonic is the dominant one in Eq. (1), here we simply take $U_{bm} = U_{1\infty}$ in calculating ψ_{wmd}.

In this study, we have two types of sand, i.e., medium sand ($d_{50} = 0.24\ mm$) and coarse sand ($d_{50} = 0.51\ mm$). Since our focus is on the wave shape effect, all tests have the same first-harmonic velocity amplitude and wave period: $U_{1\infty} = 1.5\ m/s$ and $T = 6.25\ s$. This will also facilitate the comparisons among tests with different nonlinear wave shape. The ψ_{wmd} values (calculated by taking $U_{bm} = U_{1\infty}$) for medium- and coarse-sand tests are 1.76 and 1.00, respectively, which are both larger than the 0.7 threshold. Three target values of the relative size of second harmonic (α in Eq. (1)) are involved in this study: $\alpha = 1/4, 1/6, 1/12$. Two target values of second-harmonic phase φ_0 are selected, i.e., $\varphi_0 = 0°$ for purely skewed oscillatory flows, and $\varphi_0 = 90°$ for purely asymmetric oscillatory flows. Thus, totally six different flows are involved in this study, which are presented in Fig. 2. Apparently, larger α value gives more significant nonlinear feature.

Totally 23 tests with coarse sand and 26 tests with medium sand were conducted, which covers bottom slope from 0° to 2.5°. Table 1 summarizes the coarse-sand tests, and Table 2 summarizes the medium-sand tests. Some tests are also repeated to check the reliability. The test identifier (ID) are designed to include key information of test condition. For example, in "CSKa_S25", 'C' refers to the coarse sand (changed to 'M' for medium sand)

'SK' means the skewed wave shape, 'a' denotes the level of nonlinearity (a, b, c for target α=1/4, 1/6 and 1/12, respectively), and 'S25' means that the slope is 2.5°. Similar to some previous sheet-flow OWT experiments (e.g. Watanabe and Sato, 2004; Ruessink et al., 2011), the duration of our tests is about 20-30 flow periods. The actual piston movement was recorded and converted to actual flow conditions. The obtained values for $U_{1\infty}$, α and φ_0 are presented in Tables 1 and 2. The first harmonic was very precisely produced, and the second-harmonic amplitude ($\alpha U_{1\infty}$ value) was produced with an inaccuracy of O(1%). The error for producing second-harmonic phase (φ_0) is a few degrees, except for one test ("CSKc_S00"). Since the bottom-slope effect will be studied by comparing two tests with the same target flow but different bottom slope, the influence of imperfect flow generation must be carefully considered, which will be addressed in section 3.2.

2.3. Measurement of net sediment transport rate

For each test, the LBP system gives measurements of bed elevation change Δz_b for the whole movable bed between the two boundaries denoted as $x = x_0 = 95\ mm$ and $x = x_L = 8905\ mm$ (see Fig. 1). Here the positive x-direction is the direction in which the flow is enhanced by the wave nonlinearity, which can also be considered as the "onshore" direction. In all test, the downslope direction is always in the negative x-direction or "offshore" direction. The volumes of sediment deposited outside the two boundaries ($x = x_0$ and x_L) were collected, which are denoted as V_0 (at x_0 end) and V_L (at x_L end), respectively. These measurements are subsequently used to determine the net sediment transport rate q_s along the test section based on

the principle of sand volume conservation, i.e.

$$q_s(x) = -\frac{1-\varepsilon}{\Delta T}\int_{x_0}^{x}\left[\Delta z_b(x) + \delta z\right] dx - \frac{V_0}{\Delta T b} \tag{4}$$

where x is the longitudinal coordinate, ΔT is test duration, b is the channel width, ε is sediment porosity (0.482 for coarse sand and 0.424 medium sand according to YLM17). Notice that a correction δz is added to the measured bed elevation change Δz_b, which is given by

$$\delta z = \frac{V_{LBP} - (V_0 + V_L)}{(1-\varepsilon)(x_L - x_0)b} \tag{5}$$

where

$$V_{LBP} = -(1-\varepsilon)b\int_{x_0}^{x_L}\Delta z_b(x)dx \tag{6}$$

is the loss of sand volume inside the test section. This correction was proposed by YLM17 for correcting the bed elevation change due to a slight flow-induced bed compaction, which makes $V_{LBP} - (V_0 + V_L)$ positive (a zero value is enforced by volume conservation).

Fig. 3 shows the results for two typical tests, "MSKb_S00" and "MSKb_S25". Both tests have skewed oscillatory flows with the target second harmonic being 1/6 of the first harmonic. Both tests have positive (or onshore) net transport rate. Thus, as shown in Fig. 3a, a scour is developed near the x_0 (offshore or downslope) end. In the middle of the test section Δz_b only fluctuates around zero, and these fluctuations are associated with the development of large-scale bedforms, which is believed to be an inevitable facility effect (see YLM17 for more discussions). As shown in Fig. 3b, the obtained $q_s(x)$ is quite uniform in the middle of the test section, except for some minor variations due to the bedform developments. Thus, a central region with

equilibrium net transport rate is confirmed, and the net transport rate q_{net} is simply taken as the spatial average of q_s (red dashed lines in Fig. 3b) within the equilibrium region (between red crosses in Fig. 3b). Since test "MSKb_S25" is on a 2.5° sloping bed, the slope effect is expected to reduce the onshore (upslope) transport rate, so it has a smaller q_{net} than test "MSKb_S00" (horizontal bed). Also because of the reduction in onshore q_{net}, the x_0-end scour is smaller for test "MSKb_S25". More discussions on experimental results will be provided in the next section.

3. Experimental Results

This section starts with a brief presentation of measured net transport rates due to nonlinear wave shape on horizontal beds, which is necessary for demonstrating the credibility of our experimental results. This will be followed by the results for sloping-bottom tests and in-depth discussions on how bottom slope affects net transport rate under skewed or asymmetric oscillatory flows.

3.1. Net sheet-flow sediment transport rate for tests over a horizontal bed

On a horizontal bed, the net transport rate q_{net} is only due to nonlinear wave shape. In this study, there are 12 tests covering two types of nonlinear wave shape (skewed or asymmetric oscillatory flows), and the relative magnitude of second-harmonic velocity (α in Eq. (1)) quantifies the nonlinearity. Thus, Fig. 4 presents the variation of q_{net} with α for the two flow types. Apparently, q_{net} increases with α (or nonlinearity) for both flow types from $O(10\ mm^2/s)$ for $\alpha = 1/12$ to $O(100\ mm^2/s)$ for $\alpha = 1/4$. Comparing the results for the two sediment grains, it is found that q_{net} of medium-sand

tests is generally larger than that for coarse-sand tests under the same flow condition, but the difference is not very pronounced (less than a factor of 2). Similar grain size effect (expect for fine sand, or $d_{50} < 0.2\,mm$) was also observed in some previous OWT experiments with similar grain sizes, e.g., O'Donoghue and Wright (2004) for skewed flows and van der A et al. (2010) for asymmetric flows.

To further check if our measurements are in agreement with previous OWT studies, here we compare our results with the predictions of the "SANTOSS" formula proposed by van der A et al. (2013). This formula follows the semi-unsteady and half-cycle concept for modeling net sediment transport rate for non-breaking waves and currents, and it is calibrated against a large dataset including most existing OWT experimental results. Therefore, the model-data agreement can be considered as a comparison between our and previous OWT studies. Fig. 5 shows the model validations for the two sediment diameters, separately. It can be seen that the formula works quite well, i.e., all predictions are within a factor of 2 from the measurements. The average agreement is a factor of 1.03 for coarse-sand tests and 0.84 for medium-sand tests. This good model-data agreement shows that our experimental results on nonlinear-wave-shape effect are comparable to similar previous studies.

3.2. Net sheet-flow transport rate for tests over sloping beds

Fig. 6 presents the variation of net transport rate q_{net} with bottom slope β for each flow-sediment condition. Apparently, q_{net} decreases with β. This is because the downslope direction is the "offshore" direction for all tests, so the bottom-slope effect decreases the "onshore" or positive net transport rate

due to nonlinear wave shape. For tests with the weakest wave nonlinearity, i.e. the 'c'-class tests (e.g. "MSKc"), q_{net} can be reduced to almost zero for $\beta = 2.5°$.

We can have a preliminary assessment of the slope effect by comparing the trend lines given by connecting the measured q_{net} data points for each flow-sediment condition. In each sub-figure of Fig. 6, the trend lines are more-or-less parallel, indicating that the slope effect appears insensitive to the degree of nonlinearity. Meanwhile, for tests with same sediment but different flow types it seems that the rate at which q_{net} decreases with β are also fairly similar, e.g., the two groups of trend lines in Fig. 6c and Fig. 6d appear parallel. These observations suggest that the slope effect may be independent of the wave shape effect. The second preliminary remark is that many trend lines seem reasonably straight, e.g. the "MSKa" tests in Fig. 6c, which suggests that the slope's contribution in net transport rate varies linearly with bottom slope. These two remarks will be further examined in the following sub-sections.

3.3. Evaluation of bottom-slope effect

For each sloping-bed test, the slope's contribution of net transport rate Δq can be evaluated through

$$\Delta q = -(q_{net} - q_{net,0}) \tag{7}$$

where $q_{net,0}$ is the net transport rate of the test with the same flow-sediment condition but on a horizontal bed, and the minus sign is introduced to make Δq positive. For instance, $\Delta q = 35.23\ mm^2/s$ for test "MSKa_S25" is obtained with its $q_{net} = 103.71\ mm^2/s$ and $q_{net,0} = 138.94\ mm^2/s$ (of

"MSKa_S00"). The results are presented in Table 3. The data confirms that Δq increases with β, as suggested by Fig. 6.

A key requirement for applying Eq. (7) is that the flow condition must be identical for the two involved tests, which is specially important when the bottom slope effect is relatively weak. Otherwise, Δq would just reflect the difference in flow generation. As introduced in section 2.2 (Table. 1 and 2), the actual flow conditions are slightly different from the target, so it is necessary to assess whether this will contribute substantially to the obtained Δq. Since this cannot be achieved experimentally, we applied the "SANTOSS" model (van der A et al., 2013) to evaluate the difference in net transport rate (denoted as Δq_{flow}) due to slight difference in flow conditions. As mentioned before, this model is calibrated against a wide range of OWT experiments with skewed or asymmetric oscillatory flows, and in section 3.1 we showed that the model works well for our horizontal bed tests. Using this model and the actual flow conditions reported in Table 1 and 2, q_{net} due to nonlinear wave shape is predicted for a pair of test involved in calculating Δq through Eq. (7), so the difference Δq_{flow} is

$$\Delta q_{flow} = q_{p,2} - q_{p,1} \tag{8}$$

where $q_{p,1}$ and $q_{p,2}$ are the predictions of net transport rate with $\beta = 0°$ and the actual flow conditions, respectively. The results for Δq and Δq_{flow} are shown in Table 3. Generally speaking, Δq_{flow} is of $O(1\ mm^2/s)$, which is usually one order of magnitude smaller than Δq, so the imperfect flow generation should not be a big concern. However, for tests with the smallest bottom slope (e.g. $\beta = 1.3°$), the majority of tests have Δq_{flow} comparable to Δq, e.g. $\mid q_{flow}/\Delta q \mid$ can be up to 256%. This is because the slope-induced

transport rate is weak for 1.3°-slope tests, so the change in q_{net} due to a slight change in flow condition becomes quite significant. Also, the influence of Δq_{flow} seems to be more significant for the coarse-sand tests. We have to admit that the overall quality of the coarse-sand tests is not so good as that of the medium-sand tests. The main reason is that the development of large-scale bedform (see Fig. 3) is much faster for the coarse-sand bed. As a result, the coarse-sand tests have shorter test duration (20 periods) than the medium-sand tests (25-30 periods), so the influence of the initial 1-2 periods, when the equilibrium stage for flow and sediment motion is not established yet, is more significant for coarse-sand tests. In the following analysis, we exclude tests with $|\Delta q_{flow}/\Delta q|$ over 50%.

The experimental error for Δq is estimated as follows. Since Δq is the difference of two independent measurements, its error can be written as

$$\varepsilon_{\Delta q} = \sqrt{2}\varepsilon_q \tag{9}$$

where ε_q is the experimental error for one measurement. Here ε_q is evaluated based on the discrepancies between repeated tests (half of the difference). As shown in Table 1 and 2, three coarse-sand tests and five medium-sand tests are repeated. The averaged discrepancy is 2.78 mm^2/s and 2.19 mm^2/s for coarse- and medium-sand tests, respectively. These values are used as ε_q, so $\varepsilon_{\Delta q}$ is 3.93 and 3.10 mm^2/s for coarse- and medium-sand tests, respectively.

3.4. Discussions

In this section, we investigate whether bottom-slope effect on q_{net} is independent of wave nonlinearity. To facilitate the discussion, the slope's con-

tribution in net sediment transport rate is normalized as

$$\Phi_\beta = \frac{\Delta q}{\sqrt{(s-1)gd_{50}}d_{50}} \tag{10}$$

Fig. 7 presents the variations of Φ_β with β for skewed and asymmetric oscillatory flows, separately. Overall speaking, a trend that Φ_β increases with β is confirmed by the data. For medium-sand tests (Fig. 7b), the data cloud of skewed-flow tests is a bit below that of asymmetric-flow tests. However, for coarse-sand tests (Fig. 7a), the data points of skewed-flow tests seems to be slightly above that of asymmetric-flow tests. For quantitative comparisons, we fit a straight line

$$\Phi_\beta = \Omega_\beta \cdot \beta \tag{11}$$

to the data points, so the gradient of the fitting, Ω_β, can be used to assess the influence of wave shape. For the medium-sand tests, Ω_β is 56.4 for asymmetric flows and 45.0 for skewed flows, while for coarse-sand tests, Φ_B is 7.2 and 10.1 for asymmetric- and skewed-flow tests, respectively. The relative difference (half of discrepancy divided by mean) is 11% and 17% for medium- and coarse-sand tests, respectively. The larger relative difference for coarse-sand tests is possibly due to higher experimental error and less acceptable data points for Δq. Nevertheless, such small discrepancies are negligible in the context of modeling sediment transport rate (a factor of 2 is taken as conventional threshold for accuracy). Therefore, we can conclude that Δq does not vary with flow type (or the waveshape). Based on this, it is meaningful to average Δq (or Φ_β) for tests with the same value of β, and use the results to check if a linear $\Phi_\beta - \beta$ relationship exists for our tests. As shown in Fig. 8, the data points, although are not very many (only 3

and 4 points), reasonably gather around the fitted straight lines (red solid lines) that go through the origin. The coefficient of determination, R^2, for the fitting are 0.76 and 0.91 for coarse- and medium-sand tests, respectively, indicating a reasonable fitting quality. The Φ_β for individual tests (the grey full cycles) are also shown in Fig. 8. It can be seen that all data points are within a factor of 2 from the fitted linear variations. Thus, the obtained linear $\Phi_\beta - \beta$ relationships, although not perfect, are still acceptable in the context of modeling net sediment transport rate.

To further support our findings, it is of interest to see if similar slope-induced q_{net} will be obtained with comparable sinusoidal oscillatory flows. To this end, we compare our measurements with the preceding study reported by YLM17, which has the same experimental setups as this study. In their tests, net sheet-flow sediment transport rate was measured for sinusoidal oscillatory flows over sloping beds. With the same flow period ($T = 6.25s$), there is one group of coarse-sand test (C1) and one group of medium-sand tests (M2) have velocity amplitude ($U_{1\infty} = 1.61\ m/s$) that is quite close to $U_{1\infty} = 1.5\ m/s$ in this study. The comparisons between the two studies can be made based on the gradient Ω_β of the linear $\Omega_\beta - \beta$ relationship. Table. 4 lists the key test information for tests C1, M1 and our coarse- and medium-sand tests. Our tests have smaller first-harmonic velocity amplitude, so the Ω_β values are naturally smaller than those of C1 and M3. To better assess the agreement, the Ω_β values of C1 and M3 are scaled by the Shields parameter ψ_{wmd} as,

$$\Omega'_\beta = \left(\frac{\psi_{wmd,2}}{\psi_{wmd,1}}\right)^{1.5} \Omega_\beta \tag{12}$$

where $\psi_{wmd,1}$ is calculated with $U_{1\infty} = 1.61\ m/s$, $\psi_{wmd,2}$ is calculated with

$U_{1\infty} = 1.5\ m/s$, and the power of 1.5 is simply based on convention of calculating bedload sediment transport rate. For the medium-sand tests, the obtained $\Omega_\beta^{'}$ is 69.5, which is 39% larger than our experimental value ($\Omega_\beta = 50.0$). For the coarse-sand tests, the obtained $\Omega_\beta^{'}$ is 8.3, which is 6% larger than our experimental value ($\Omega_\beta^{'} = 7.8$). These discrepancies are acceptable for modeling net sediment transport rate. Thus, ours and YLM17 tests together show that bottom-slope-induced net sheet-flow sediment transport rate is independent of wave nonlinearity and varies linearly with bottom slope. As such, those well-validated empirical models over a horizontal bottom (e.g. "SANTOSS" model) can be easily extended to account for a sloping bottom by adding an extra net transport rate due to an equivalent sinusoidal wave over a sloping bottom. An empirical formula for this purpose will be introduced in the next section.

4. Empirical formula for net transport rate due to slope effect

The basic formula for predicting slope-induced net sheet-flow sediment transport rate is Eq. (11). Based on the findings in section 3, the gradient Ω_β in Eq. (11) only depends on the sinusoidal flow condition and the sediment condition. Here two flow parameters, excursion amplitude (A_{bm}) and velocity amplitude (U_{bm}), are selected to represent the flow condition. Other relevant physical quantities are sediment median diameter (d_{50}), fluid viscosity (v) and the submerged gravitational acceleration $(s-1)g$. Dimensional analysis suggests that Ω_β is a function of the following three dimensionless parameters, i.e.,

$$A_\star = \frac{A_b}{d_{50}}, Re_d = \frac{\sqrt{(s-1)gd_{50}}d_{50}}{v}, \phi = \frac{U_{bm}^2}{(s-1)gd_{50}} \tag{13}$$

which are hereafter referred to as normalized excursion amplitude, particle Reynolds number and mobility number. Notice that ϕ is related to the characteristic Shields parameter ψ_{wmd} defined in Eq. (2) via

$$\psi_{wmd} = \frac{f_{wd}}{2}\phi \tag{14}$$

where the friction factor f_{wd} is only a function of $A^\star$, according to Eq. (3). Thus, we can replace ϕ by ψ_{wmd} in the following analysis. It can be expected that larger ψ_{wmd} should give larger Ω_β. Following the convention for modeling sediment transport rate, a power-law dependency on ψ_{wmd} is assumed

$$\Omega_\beta = M\left(\psi_{wmd} - \psi_{cr}\right)^N \tag{15}$$

where ψ_{cr} is the critical Shields parameter for incipient motion, and the parameters M and N are functions of $A^\star$ and Re_d. Following Zyserman and Fredsøe (1994), we simply take $\psi_{cr} = 0.045$.

A large dataset would be required to calibrate an empirical formula for M and N in Eq. (15). The only existing dataset is the one reported by YLM17. Their experiments covered 6 sinusoidal flow-sediment conditions, so only 6 experimental values of Ω_β are available, which is apparently insufficient. YLM17 also developed a process-based model for slope-induced q_{net} under sinusoidal oscillatory flows. The readers are referred to their paper for model introduction. This model can well predict the YLM17's measurements. The overall model-data agreement is a factor of 1.03 (the benchmarking involves tests with $d_{50} = 0.13\ mm$ $d_{50} = 0.24\ mm$ and $d_{50} = 0.51\ mm$), so its prediction can be treated equally as measurement. Thus, a combined model-data approach for solving the issue of insufficient calibration data is proposed

as follows. We first use the YLM17 model to generate a large dataset of predicted Ω_β that covers wide ranges for ψ_{wmd}, $A^\star$ and Re_d. The predictions are used as the database for calibrating the power N in Eq. (15). The remaining parameter M is then calibrated against the measurements of YLM17.

The predictions cover d_{50} from 0.1 to 1 mm with a 0.05 mm interval, which translates to Re_d from 4.0 ($d_{50} = 0.1$ mm) to 127.2 ($d_{50} = 1$ mm). The range of ψ_{wmd} is from 0.7 to 2 with a 0.05 interval, since 0.7 is the threshold for sheet-flow condition and 2 is already a very high value. 25 values of $A^\star$ from 500 to 30000 are selected based on a logarithmic spacing, which translates to $A_{bm} \sim 5$ cm to 3 m for $d_{50} = 0.1$ mm and $A_{bm} \sim 50$ cm to 30 m for $d_{50} = 1$ mm. The YLM17 model is applied to predict Ω_β with any combination of $A^\star$, Re_d and ψ_{wmd}. It is found that the variation of N with sediment diameter (or Re_d) is insignificant, so for simplicity N is assumed to be a single-value function of $A^\star$, The following equation of N is obtained by data fitting:

$$N = \begin{cases} 1.5, & A^\star \leq 500 \\ 0.1710 \ln(A^\star) + 0.4375, & 500 < A^\star \leq 30000 \\ 2.2, & A^\star > 30000 \end{cases} \tag{16}$$

For a given d_{50} (or Re_d), smaller value of excursion amplitude is associated with thinner wave boundary layer, which indicates weaker sediment suspension. Therefore, for very low value of $A^\star$, the sediment transport can be considered as dominantly bedload. Note that the power N is 1.5 in the widely used Meyer-Peter-Müller bedload formula, which is also the value we obtained for $A^\star \leq 500$. For large value of $A^\star$, suspended load becomes increasingly important, so N becomes larger.

The parameter M is found to increase with $A^\star$, but decreases with Re_d, so M is taken as a function of a combined parameter $\sqrt{A^\star/Re_d}$. Using the values of Ω_β derived from YLM17's measurements, six values of M are calculated with Eqs. (15) and (16), which are shown in Fig. 9. The six points give a clear trend that M increases with $\sqrt{A^\star/Re_d}$, and the increasing rate becomes negligible for $\sqrt{A^\star/Re_d} > 28$. Thus, the following three-part formula is fitted to the obtained M values

$$M = \begin{cases} 9, & \sqrt{\frac{A^\star}{Re_d}} < 8 \\ 0.0137\left(\sqrt{\frac{A^\star}{Re_d}}\right)^3 - 0.4625\left(\sqrt{\frac{A^\star}{Re_d}}\right)^2 + 5.1128\left(\sqrt{\frac{A^\star}{Re_d}}\right) & \\ -9.6565, & 8 \leq \sqrt{\frac{A^\star}{Re_d}} < 28 \\ 71, & \sqrt{\frac{A^\star}{Re_d}} \geq 28 \end{cases} \tag{17}$$

Eqs. (11), (15), (16) and (17) together define an empirical model that predicts sheet-flow q_{net} due to bottom slope effect.

As suggested in previous discussions, the proposed empirical model can be added to "SANTOSS" model to account for slope effect under skewed or asymmetric flows. "SANTOSS" model predicts net transport rate due to flow nonlinearity, while the proposed empirical formula calculate the slope-induced net transport rate under equivalent sinusoidal flows, which are determined by equating the root-mean-square velocity (u_{rms}) to associated skewed or asymmetric flows, where the amplitude is

$$u_{bm} = \sqrt{\frac{2}{T}\int_0^T U_\infty^2(t)dt} \tag{18}$$

In our tests, flow nonlinearity and bottom slope coexist, so they are appropriate for evaluating the performance of combined "SANTOSS" and the empirical model. The results are given in Fig. 10a. Generally speaking, the

combined model performs very well in terms of predicting net transport rates, with an overall agreement of a factor of 0.94 (dashed line). Only 3 medium-sand tests are outside the thresholds of a factor of 2. These are tests with a 1.3° slope, so nonlinear-wave and slope effect cancel each other, leading to a small net transport rate. Notably, prediction error becomes higher when the quantity is close to zero. To better assess if the empirical model captures the slope effect adequately, the predicted slope's contribution in net transport rates are compared with measurements reported in Table. 3, and the results are shown in Fig. 10b. Note that the questionable data points due to large imperfect-flow generation (indicated as $|\Delta q_{flow}|/\Delta q_{net,\beta} > 50\%$) are also excluded in the model-data comparison for Δq. The darkness of the symbols increases with bottom slope. The inaccuracy of all the predictions are within a factor of 2, and the overall agreement is also quite good (a factor of 1.11) in terms of modeling net sediment transport rate. Consequently, the combined model is applicable to scenarios with sloping bottoms and nonlinear flows.

5. Conclusions

Experiments of sheet-flow sediment transport under oscillatory flows with nonlinear wave shape were conducted in an inclinable OWT, so the effect of bottom slope on net transport rate q_{net} in the context of nonlinear waves is experimentally investigated. The tests cover two wave shapes (skewed and asymmetric oscillatory flows), two sediment diameters (0.24 mm and 0.51 mm) and bottom slope up to 2.5°. All tests have the same first-harmonic velocity and flow period, so they have the same primary oscillatory flow. A laser-based bottom profiler is applied to measure the change of movable

bed, which is used to estimate q_{net} based on the principle of sand volume conservation.

For tests on horizontal beds, a positive or "onshore" q_{net} is observed for all tests, which increases with the degree of wave nonlinearity. A good model-data agreement between our measurements and the empirical formula proposed by van der A et al. (2013) is obtained, which suggests that our tests are similar to those OWT studies in the model's calibration dataset. Since the downslope direction in the sloping-bottom tests is the negative or "offshore" direction, it is observed that q_{net} under the same flow-sediment condition decreases with increasing bottom slope. For some tests, the slope-induced net offshore transport rate almost cancels the nonlinearity-induced net onshore transport rate.

For each sloping-bed test, bottom slope's contribution to net transport rate, Δq, is estimated by subtracting q_{net} of its corresponding horizontal-bed test. It is noticed that the actual flow deviated slightly from the target, which may contribute to the obtained Δq. This issue is estimated to be insignificant with empirical model of van der A et al. (2013), but a small number of tests suffer substantially from imperfect-flow generation are identified and excluded in the subsequent analysis. For a given slope and sediment diameter, there is little difference in Δq between skewed-flow and asymmetric-flow tests. Thus, we conclude that net sheet-flow transport rate associated with bottom slope is insensitive to wave nonlinearity. A linear relationship between Φ_β (normalized Δq) and β, i.e. $\Phi_\beta = \Omega_\beta \cdot \beta$, is fitted to both coarse-sand and medium-sand tests. Although the data points do not closely follow the linear fits, the discrepancies are all within a factor of 2. Thus, in the context of

modeling sediment transport, this simple linear dependency is acceptable. The obtained values of Ω_β also agree well with those from sinusoidal-flow tests of YLM17. Thus, our experimental results imply that net sheet-flow transport rate under nonlinear shoaling waves over a sloping bed can be modeled as the superposition of two net transport rates, one is due to nonlinear waves over a horizontal bed and the other is due to an equivalent linear wave (sinusoidal oscillatory flows) over a sloping bed. This is the key finding of our study, which was also suggested by Yuan and Tan (2018) through their model applications.

A new empirical formula is therefore developed for predicting q_{net} due to bottom slope. Following $\Phi_\beta = \Omega_\beta \cdot \beta$, it is only necessary to obtain formula for Ω_β. A dimensional analysis suggests that Ω_β depends on three dimensionless parameter, namely the normalized excursion amplitude $A^\star = A_b/d_{50}$, a characteristic Shields parameter ψ_{wmd}, and a particle Reynolds number $Re_d = \sqrt{(s-1)gd_{50}}d_{50}/v$. Following the convention for modeling sediment transport rate, a power-law relationship between Ω_β and $(\psi_{wmd} - \psi_{cr})$ is assumed, i.e. $\Omega_\beta = M(\psi_{wmd} - \psi_{cr})^N$. A combined model-data approach is adopted to calibrate empirical formulas for the two parameters M and N. More specifically, N is calibrated against a large dataset predicted by the simple process-based YLM17 model, while the parameter M is calibrated against measurements of YLM17. As a demonstration, the newly calibrated model for slope effect is combined with the "SANTOSS" model for wave nonlinearity. The combined model is applied to the tests in this study. The model-data comparison shows a good overall agreement, which confirms the key finding of this research.

Acknowledgments

The authors gratefully acknowledge the financial support from the Tier-1 research project funded by the Ministry Of Education of Singapore (WBS: R-302-000-126-112).

References

van der A, D.A., O'Donoghue, T., Ribberink, J.S., 2010. Measurements of sheet flow transport in acceleration-skewed oscillatory flow and comparison with practical formulations. Coastal Engineering 57, 331–342.

van der A, D.A., Ribberink, J.S., van der Werf, J.J., O'Donoghue, T., Buijsrogge, R.H., Kranenburg, W.M., 2013. Practical sand transport formula for non-breaking waves and currents. Coastal Engineering 76, 26–42.

Bailard, J., 1981. An energetics total load sediment transport model for a plane sloping beach. Journal of Geophysical Research: Oceans 86, 10938–10954.

Caliskan, U., Fuhrman, D.R., 2017. Rans-based simulation of wave-induced sheet-flow transport of graded sediments. Coastal Engineering 121, 90–102.

Chen, X., Li, Y., Niu, X., Chen, D., Yu, X., 2011. A two-phase approach to wave-induced sediment transport under sheet flow conditions. Coastal Engineering 58, 1072–1088.

Davies, A.G., Li, Z., 1997. Modelling sediment transport beneath regular symmetrical and asymmetrical waves above a plane bed. Continental Shelf Research 17, 555–582.

Davies, A.G., Soulsby, R.L., King, H.L., 1988. A numerical model of the combined wave and current bottom boundary layer. Journal of Geophysical Research: Oceans 93, 491–508.

Dohmen-Janssen, C.M., Kroekenstoel, D.F., Hassan, W.N., Ribberink, J.S., 2002. Phase lags in oscillatory sheet flow: experiments and bed load modelling. Coastal Engineering 46, 61–87.

Fuhrman, D.R., Schløer, S., Sterner, J., 2013. RANS-based simulation of turbulent wave boundary layer and sheet-flow sediment transport processes. Coastal Engineering 73, 151–166.

Gonzalez-Rodriguez, D., Madsen, O.S., 2007. Seabed shear stress and bedload transport due to asymmetric and skewed waves. Coastal Engineering 54, 914–929.

Hassan, W.N.M., Ribberink, J.S., 2010. Modelling of sand transport under wave-generated sheet flows with a rans diffusion model. Coastal Engineering 57, 19–29.

Hsu, T.J., Jenkins, J.T., Liu, P.L.F., 2004. On two-phase sediment transport: sheet flow of massive particles, in: Proceedings of the Royal Society of London A: Mathematical, Physical and Engineering Sciences, The Royal Society. pp. 2223–2250.

Humbyrd, C.J., 2012. Turbulent combined wave-current boundary layer model for application in coastal waters. Master's thesis. Massachusetts Institute of Technology. Cambridge, MA, U.S.

King, D.B., 1991. Studies in oscillatory flow bedload sediment transport. Ph.D. thesis. University of California. San Diego, CA, U.S.

Kranenburg, W.M., Ribberink, J.S., Uittenbogaard, R.E., Hulscher, S.J.M.H., 2012. Net currents in the wave bottom boundary layer: On waveshape streaming and progressive wave streaming. Journal of Geophysical Research 117, F03005.

Liu, H., Sato, S., 2006. A two-phase flow model for asymmetric sheetflow conditions. Coastal Engineering 53, 825–843.

Longuet-Higgins, M.S., 1953. Mass transport in water waves. Philosophical Transactions of the Royal Society of London. Series A, Mathematical and Physical Sciences 245, 535–581.

Madsen, O.S., 1993. Sediment transport outside the surf zone. Technical Report U.S. Army Engineer Waterways Experiment Station.

Madsen, O.S., Grant, W.D., 1977. Quantitative description of sediment transport by waves. Proc. 15th Int. Coastal Eng. Conf., ASCE , 1093–1112.

Nielsen, P., 1992. Coastal Bottom Boundary Layers and Sediment Transport. World Scientific Publishing.

O'Donoghue, T., Wright, S., 2004. Flow tunnel measurements of velocities and sand flux in oscillatory sheet flow for well-sorted and graded sands. Coastal Engineering 51, 1163–1184.

Ribberink, J.S., 1998. Bed-load transport for steady flows and unsteady oscillatory flows. Coastal Engineering 34, 59–82.

Ribberink, J.S., Al-Salem, A.A., 1995. Sheet flow and suspension of sand in oscillatory boundary layers. Coastal Engineering 25, 205–225.

Ruessink, B.G., van den Berg, T.J.J., van Rijn, L.C., 2009. Modeling sediment transport beneath skewed asymmetric waves above a plane bed. Journal of Geophysical Research: Oceans 114, C11.

Ruessink, B.G., Michallet, H., Abreu, T., Sancho, F., Van der A, D.A., Van der Werf, J.J., Silva, P.A., 2011. Observations of velocities, sand concentrations, and fluxes under velocity-asymmetric oscillatory flows. Journal of Geophysical Research: Oceans 116.

da Silva, P.A., Temperville, A., Seabra Santos, F., 2006. Sand transport under combined current and wave conditions: A semi-unsteady, practical model. Coastal Engineering 53, 897–913.

Trowbridge, J., Madsen, O.S., 1984. Turbulent wave boundary layers: 2. second-order theory and mass transport. Journal of Geophysical Research: Oceans 89, 7999–8007.

Wang, Y.H., 2007. Formula for predicting bedload transport rate in oscillatory sheet flows. Coastal Engineering 54, 594–601.

Watanabe, A., Sato, S., 2004. A Sheet-Flow Transport Rate Formula for Asymmetric, Forward-Leaning Waves and Currents. World Scientific Publishing Company. pp. 1703–1714.

Van der Werf, J.J., Schretlen, Jolanthe, J.L.M., Ribberink, J.S., O'Donoghue, T., 2009. Database of full-scale laboratory experiments on wave-driven sand transport processes. Coastal Engineering 56, 726–732.

Yuan, J., Dongxu, W., Madsen, O.S., 2017a. A laser-based bottom profiler system for measuring net sediment transport rates in an oscillatory water tunnel. Coastal Dynamics 2017 Coastal Dynamics 2017 Paper No. 088.

Yuan, J., Li, Z., Madsen, O.S., 2017b. Bottom-slope-induced net sheet-flow sediment transport rate under sinusoidal oscillatory flows. Journal of Geophysical Research: Oceans 122, 236–263.

Yuan, J., Madsen, O.S., 2014. Experimental study of turbulent oscillatory boundary layers in an oscillating water tunnel. Coastal Engineering 89, 63–84.

Yuan, J., Madsen, O.S., 2015. Experimental and theoretical study of wave–current turbulent boundary layers. Journal of Fluid Mechanics 765, 480–523.

Yuan, J., Tan, W., 2018. Modeling net sheet-flow sediment transport rate under skewed and asymmetric oscillatory flows over a sloping bed. Coastal Engineering 136, 65–80.

Zyserman, J., Fredsøe, 1994. Data analysis of bed concentration of suspended sediment. Journal of Hydraulic Engineering 120, 121–1042.

Figure captions

Figure 1: 3D sketch of the inclinable oscillatory water tunnel.

Figure 2: Target oscillatory flows with nonlinear features: (a) purely skewed oscillatory flow, (b) purely asymmetric oscillatory flow (the α value in the legend is the relative magnitude of second-harmonic, c.f. Eq. 1).

Figure 3: Net sediment transport rate along the test channel: (a) change of bottom profile, (b) net sediment transport rate (solid lines are for test "MSKb_S00", dashed lines are for test "MSKb_S25". The red crosses in figure define the equilibrium region, which gives the net transport rate denoted by red dashed lines).

Figure 4: Net sediment transport rate for tests over horizontal bed varying with different flow nonlinearity, indicated by α in Eq. (1).

Figure 5: Comparisons of net transport rate obtained from horizontal bed tests with associated "SANTOSS" prediction (overall agreement, 1.07 and 0.98). Solid line refers to a perfect match, dot lines refer to a factor of 2.

Figure 6: Variation of net sheet-flow sediment transport rate with bottom slope. Data points are linked by dashed lines. In each sub figure, a, b, c represent the value of α $(1/4, 1/6, 1/12)$ in Eq. (1).

Figure 7: Normalized bottom-induced net sediment transport rate under skewed or asymmetric flows: (a) all coarse-sand tests, (b) all medium-sand tests. Error bars are calculated based on repeating tests. In each sub figure, black dashed line is fitting line for skewed-flow tests(slope is 12.0 in (a), 49.1 in (b)), while red solid is fitting line for asymmetric-flow tests (slope is 7.1 in (a), 51.8 in (b)).

Figure 8: Linear fitting for net sediment transport rate due to bottom slope effect (the red solid line is the linear fitting, black dashed line indicates two standard deviations from the fitting). Grey circles are data points, while solid triangles are mean values averaged over the data points on the same bottom slope.

Figure 9: Fitting the parameter M to data derived based on measurements of YLM17.

Figure 10: Validation of model combination ("SANTOSS" model and the empirical model) in predicting net sediment transport rates. (a) total net transport rate; (b) slope-induced net transport rate. The overall agreement is a factor of 0.94 for the total q_{net}, and 1.11 for slope effect. Solid circles are coarse sand tests, solid triangles are medium sand tests.

Table 1: Summary of coarse-sand tests

Test ID	$U_{1,\infty}$ [m/s]	$\alpha U_{1,\infty}$ [m/s]	$\varphi_0[^\circ]$	$\beta[^\circ]$	$q_{net}(10^{-6}m^2/s)$
CSKa_S00	1.501	0.375	8.61	0	105.98
CSKb_S00	1.501	0.251	-4.10	0	82.86
CSKc_S00	1.500	0.125	20.89	0	45.79
CASa_S00(1)	1.498	0.396	83.82	0	51.37
CASa_S00 (2)	1.498	0.385	86.68	0	48.59
CASb_S00	1.499	0.268	86.90	0	29.50
CASc_S00	1.500	0.134	83.89	0	22.26
CSKa_S25	1.502	0.379	-9.52	2.5	70.00
CSKb_S25 (1)	1.501	0.253	-7.14	2.5	62.61
CSKb_S25 (2)	1.501	0.251	-7.16	2.5	72.68
CSKc_S25	1.500	0.124	-7.76	2.5	15.55
CASa_S25 (1)	1.497	0.389	85.69	2.5	30.11
CASa_S25 (2)	1.497	0.389	85.70	2.5	26.42
CASb_S25	1.498	0.260	86.21	2.5	17.49
CASc_S25	1.499	0.128	87.76	2.5	1.90
CSKc_S20	1.501	0.127	-4.69	2	25.88
CASa_S20	1.499	0.394	83.12	2	41.91
CASb_S18	1.500	0.264	84.42	1.8	22.55
CSKa_S13	1.497	0.396	-5.68	1.3	98.50
CASa_S13	1.498	0.377	85.81	1.3	46.88

Table 2: Summary of medium-sand tests

Test ID	$U_{1,\infty}$ [m/s]	$\alpha U_{1,\infty}$ [m/s]	$\varphi_0[^\circ]$	$\beta[^\circ]$	$q_{net}(10^{-6}m^2/s)$
MSKa_S00	1.500	0.381	-3.15	0	138.94
MSKb_S00(1)	1.500	0.251	-3.03	0	93.23
MSKb_S00 (2)	1.500	0.250	-6.63	0	94.69
MSKc_S00	1.500	0.124	-4.74	0	52.09
MASa_S00	1.497	0.404	82.28	0	73.77
MASb_S00	1.499	0.270	83.02	0	51.87
MASc_S00 (1)	1.500	0.136	88.00	0	22.33
MASc_S00 (2)	1.500	0.142	84.83	0	24.16
MSKa_S25	1.501	0.380	-7.44	2.5	103.71
MSKb_S25 (1)	1.501	0.253	-8.03	2.5	65.61
MSKb_S25 (2)	1.501	0.252	-4.94	2.5	66.55
MSKc_S25	1.501	0.123	-5.82	2.5	19.993
MASa_S25 (1)	1.500	0.398	86.42	2.5	26.36
MASa_S25 (2)	1.496	0.404	82.12	2.5	36.47
MASb_S25	1.500	0.265	87.06	2.5	5.22
MASc_S25 (1)	1.499	0.139	86.89	2.5	-3.37
MASc_S25 (2)	1.500	0.135	85.98	2.5	4.16
MSKb_S20	1.501	0.253	-5.47	2.0	67.10
MSKc_S20	1.502	0.125	-3.34	2.0	20.31
MASa_S20	1.497	0.408	83.20	2.0	42.60
MASb_S20	1.499	0.270	82.31	2.0	26.07
MSKa_S13	1.501	0.383	-5.65	1.3	120.83
MSKb_S13	1.501	0.256	-2.46	1.3	81.95
MASc_S13	1.500	0.145	82.21	1.3	18.48

Table 3: Slope-induced net sheet-flow transport rate

Test ID	$\beta[^\circ]$	Δq	Δq_{flow}	$\lvert\Delta q_{flow}\rvert/\Delta q_{net,\beta}$
CSKa_S25	2.5	35.98	28.2	78%
CSKb_S25	2.5	20.25	2.47	12%
CSKc_S25	2.5	30.24	6.53	22%
CASa_S25	2.5	21.26	3.06	14%
CASb_S25	2.5	12.01	0.70	6%
CASc_S25	2.5	20.37	3.55	17%
CSKc_S20	2	19.91	4.33	22%
CASa_S20	2	9.46	-0.38	4%
CASb_S18	1.8	6.95	-1.96	28%
CSKa_S13	1.3	7.48	19.13	256%
CASa_S13	1.3	4.49	5.25	117%
MSKa_S25	2.5	35.23	8.27	23%
MSKb_S25	2.5	27.62	4.30	16%
MSKc_S25	2.5	32.10	0.66	2%
MASa_S25	2.5	47.41	4.51	10%
MASb_S25	2.5	46.65	5.03	11%
MASc_S25	2.5	25.70	-1.21	5%
MSKb_S20	2	26.13	1.63	6%
MSKc_S20	2	31.78	-0.94	3%
MASa_S20	2	31.17	0.13	0%
MASb_S20	2	25.80	-0.72	3%
MSKa_S13	1.3	18.11	4.38	24%
MSKb_S13	1.3	11.28	-2.13	19%
MASc_S13	1.3	3.85	-5.49	143%

Table 4: Comparisons between this study and Yuan et al. (2017b)

Test ID	d_{50}	$U_{1\infty}[m/s]$	T[s]	ψ_{wmd}	Ω_β
C1	0.51	1.61	6.25	1.13	10.0
Coarse sand	0.51	1.5	6.25	1	7.8
M3	0.24	1.61	6.25	2	83.7
Medium sand	0.24	1.5	6.25	1.76	50.0

Figure 1:

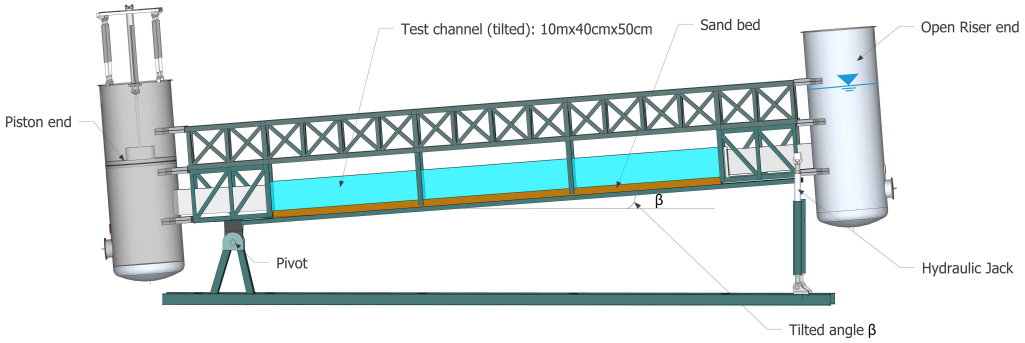

Figure 2:

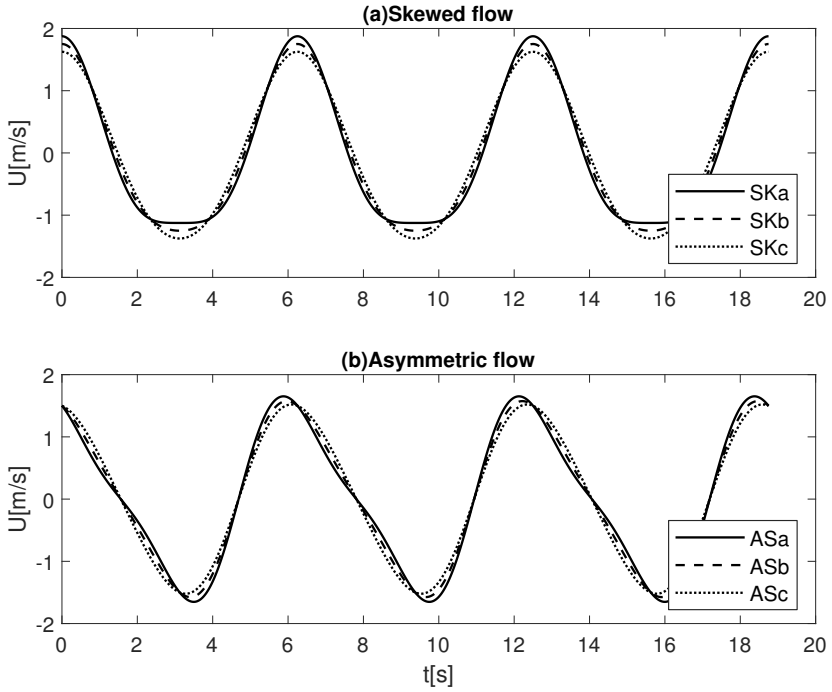

Figure 3:

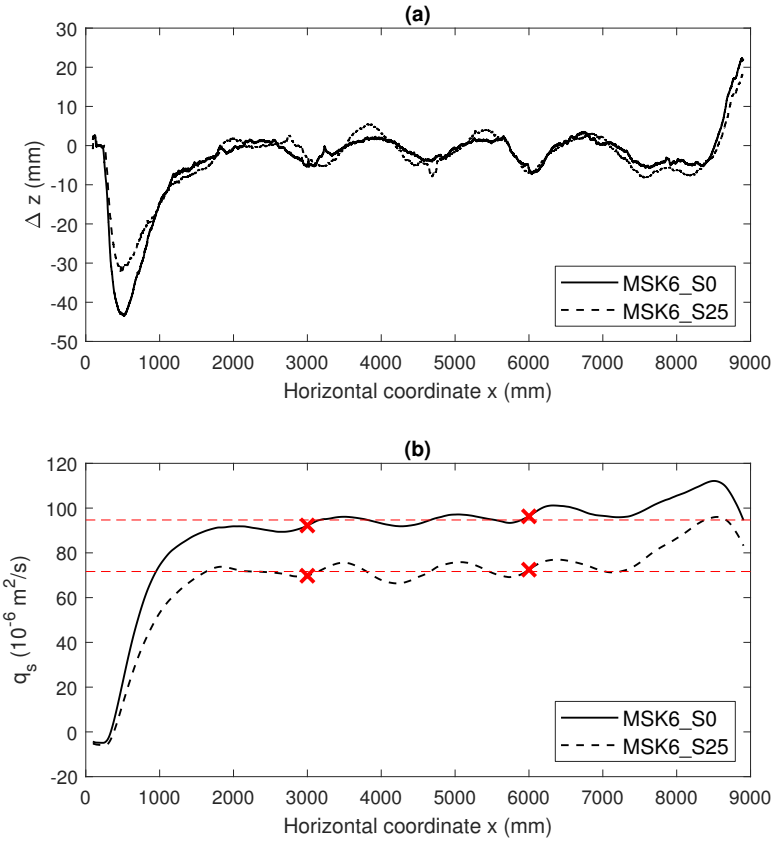
(a)
Δ z (mm)
Horizontal coordinate x (mm)
MSK6_S0
MSK6_S25
(b)
q_s (10^{-6} m^2/s)
Horizontal coordinate x (mm)
MSK6_S0
MSK6_S25

Figure 4:

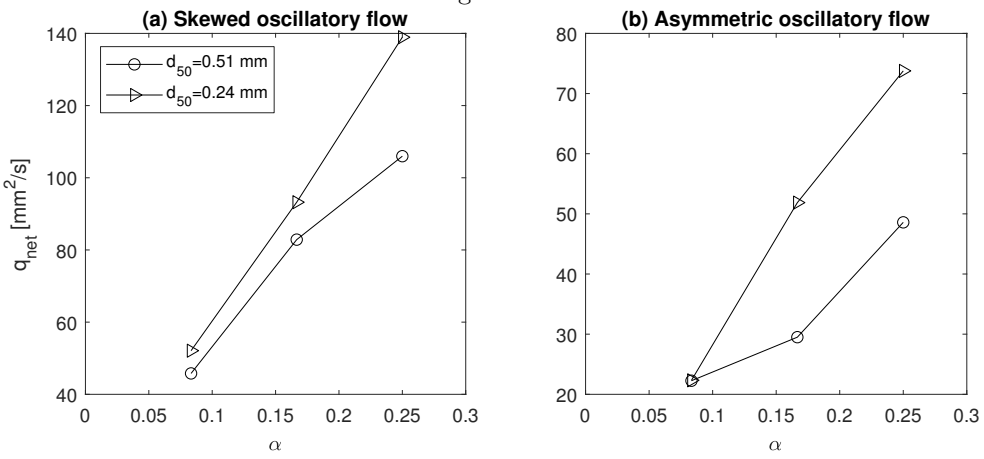
(a) Skewed oscillatory flow
d50=0.51 mm
d50=0.24 mm
qnet [mm2/s]
α
(b) Asymmetric oscillatory flow
α

Figure 5:

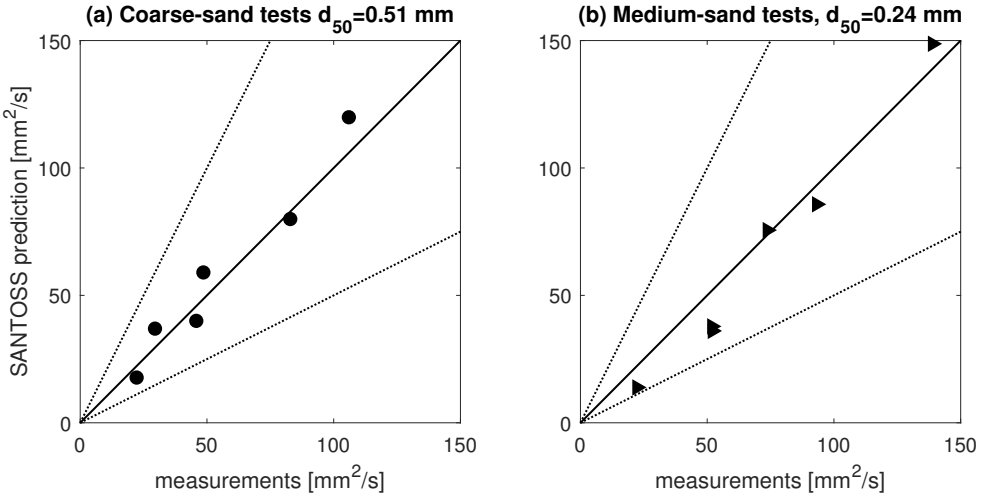
(a) Coarse-sand tests d50=0.51 mm
(b) Medium-sand tests, d50=0.24 mm
SANTOSS prediction [mm2/s]
measurements [mm2/s]
measurements [mm2/s]
0
50
100
150

Figure 6:

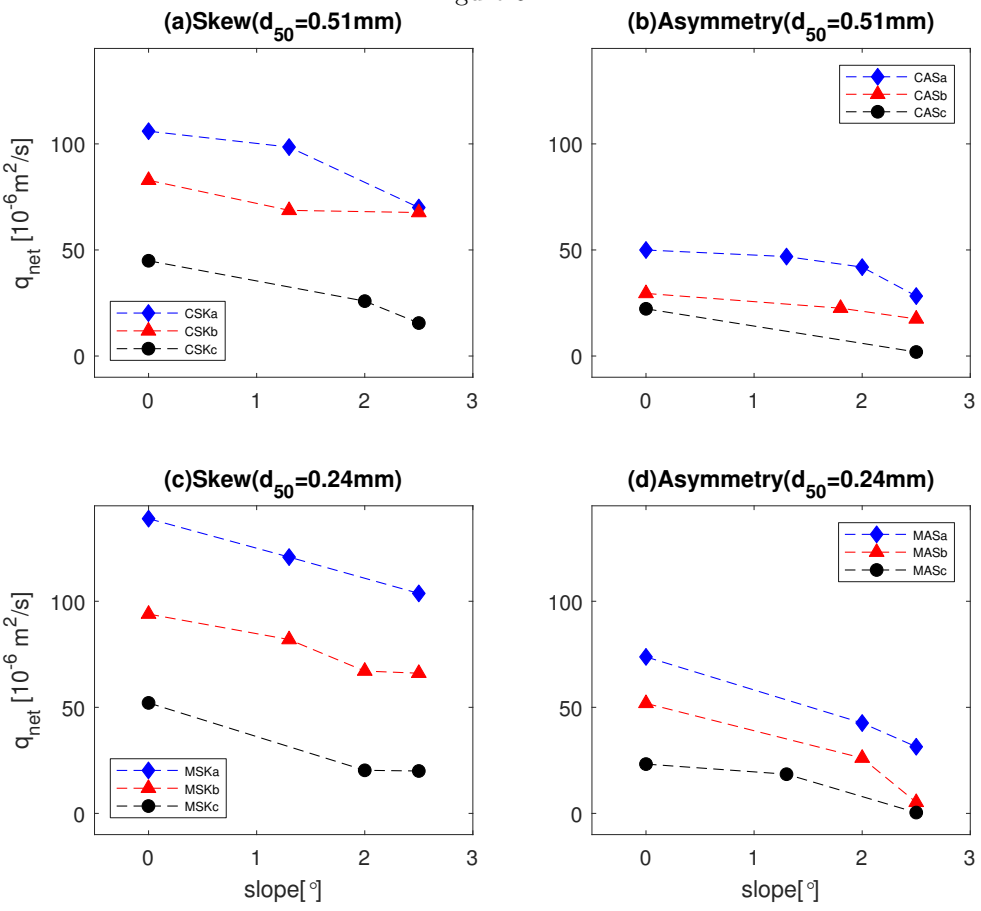
(a)Skew(d_{50}=0.51mm)
(b)Asymmetry(d_{50}=0.51mm)
(c)Skew(d_{50}=0.24mm)
(d)Asymmetry(d_{50}=0.24mm)
q_{net} [10^{-6} m^2/s]
slope[°]
CSKa
CSKb
CSKc
CASa
CASb
CASc
MSKa
MSKb
MSKc
MASa
MASb
MASc
0
50
100
0
1
2
3

Figure 7:

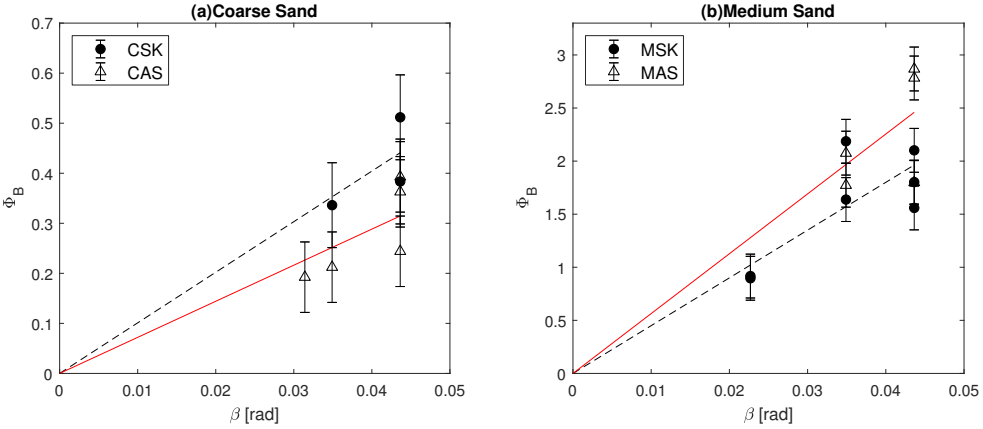
(a)Coarse Sand
CSK
CAS
Φ_B
β [rad]
(b)Medium Sand
MSK
MAS
Φ_B
β [rad]

Figure 8:

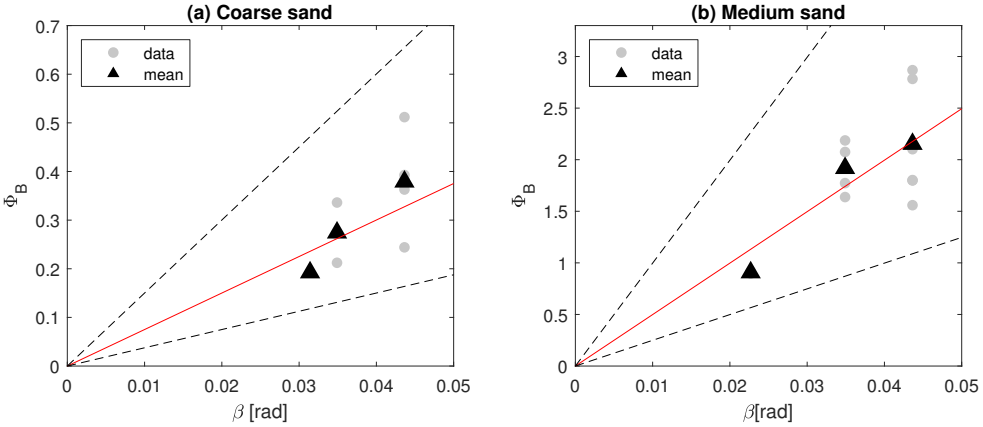
(a) Coarse sand
data
mean
Φ_B
β [rad]
0
0.01
0.02
0.03
0.04
0.05
0.1
0.2
0.3
0.4
0.5
0.6
0.7
(b) Medium sand
data
mean
Φ_B
β[rad]
0.5
1
1.5
2
2.5
3

Figure 9:

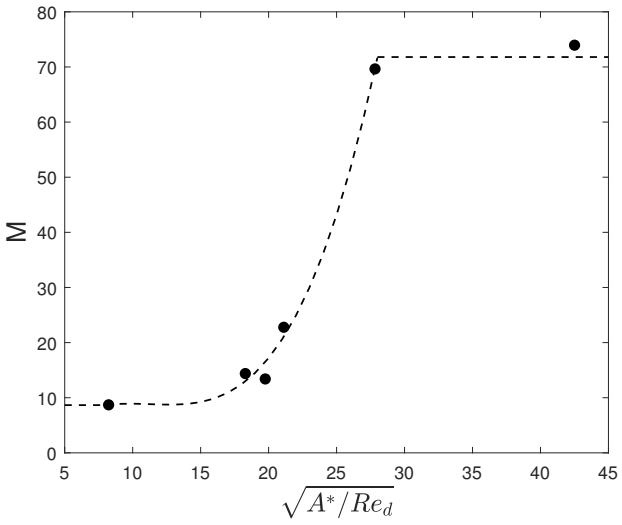

Figure 10:

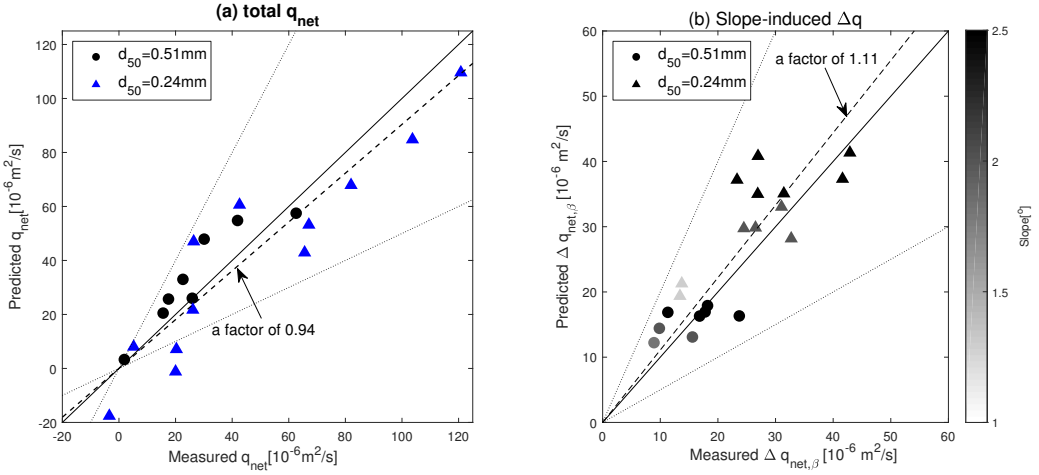
(a) total q_{net}
d_{50}=0.51mm
d_{50}=0.24mm
a factor of 0.94
Predicted q_{net}[10^{-6} m^2/s]
Measured q_{net}[$10^{-6}m^2$/s]
(b) Slope-induced Δq
d_{50}=0.51mm
d_{50}=0.24mm
a factor of 1.11
Predicted Δ $q_{net,\beta}$ [10^{-6} m^2/s]
Measured Δ $q_{net,\beta}$ [10^{-6} m^2/s]
Slope[°]